Fragility curves for existing reinforced concrete buildings, including soil-structure interaction and site amplification effects

Dimitris Pitilakis[a,*], Christos Petridis[a]

[a] Department of Civil Engineering, Aristotle University of Thessaloniki, Aristotle University of Thessaloniki, Thessaloniki, GR-54124, Greece

ARTICLE INFO

Keywords:
fragility curves
vulnerability assessment
seismic risk
site amplification
soil-structure interaction
fragility modifiers
nonlinear soil

ABSTRACT

SSI and site amplification effects are investigated as influences on the seismic fragility of existing reinforced concrete moment-resisting frame and dual frame-wall system buildings supported on shallow foundations without interconnecting beams. We build upon a holistic methodology that accounts for site amplification and soil-foundation-structure interaction effects using a modular approach. We calculate fragility curves based on nonlinear dynamic analyses for various building structural typologies and geometries, infill conditions, code provisions, and soil profile materials and dynamic characteristics. We demonstrate that site amplification during earthquakes may significantly increase the fragility of the soil-foundation-structure system, which is reflected in its vulnerability. Moreover, SSI is especially prevalent for buildings on soft soil profiles and might modify their fragility. We propose a modular method to include site amplification and/or soil-structure interaction effects in a large-scale earthquake vulnerability assessment using fragility modifiers, which we express using an easy-to-code equation form.

1. Introduction

Earthquakes pose a severe threat to societies, and always the effort has been directed toward quantifying and mitigating expected damage and loss. In the last few years, vulnerability and fragility curves have become a critical tool for various purposes associated with earthquake risk management and resilience, including estimation of earthquake losses, structural design, retrofit, earthquake insurance, and business continuity. In the absence of adequate empirical data, analytical and hybrid methodologies emerged within the context of analyzing fragility and vulnerability curves (1), with the subject of discussions and improvements being at the forefront (2).

A large majority of vulnerability and risk assessment studies assume fixed-base buildings today. Although a great deal has been written regarding the influence of soil and foundations on structures (3; 4; 5), how these effects affect fragility curves remains a subject of active research, as Silva et al. (2) indicate. Tang and Zhang (6) investigated, in a probabilistic manner, the seismic demand imposed on a slender reinforced concrete (RC) shear wall based on a flexible foundation and found that soil-structure interaction (SSI) generally decreased the damage probability of the shear wall. Saez et al. (7) examined the influence of inelastic soil behavior and SSI on the seismic vulnerability assessment of structures, noting that fragility curves reflect the seismic demand reduction because of SSI. Rajeev and Tesfamariam (8) investigated the effect of SSI and soil uncertainties on fragility curves using an optimized latin hypercube sampling technique. Behnamfar and Banizadeh (9) studied the distribution of seismic vulnerability in RC buildings, comparing

*Corresponding author at Department of Civil Engineering, Aristotle University of Thessaloniki, Thessaloniki, GR-54124, Greece
dpitilakis@civil.auth.gr (D. Pitilakis); cpetridi@civil.auth.gr (C. Petridis)
ORCID(s): 0000-0001-7363-3667 (D. Pitilakis); 0000-0002-6078-1684 (C. Petridis)

fixed-base and flexible-base models. They found that the location of maximum drift shifts to the first story, where the most intensive vulnerability is observed. Karapetrou et al. (10) derived a set of fragility curves for a 9-story RC moment-resisting frame (MRF) building, including site effects and SSI. They showed that the vulnerability increases with respect to the reference fixed-base model. Pitilakis et al. (11) investigated aging and SSI effects on high-rise buildings resting on soil profiles, and concluded that vulnerability increases over time because of corrosion. Recently, Karafagka et al. (12) produced fragility curves for MRF structures, including SSI and soil liquefaction effects. Cavalieri et al. (13) used a macroelement approximation of the foundation response to include SSI effects in calculating the fragility curves of buildings. They concluded that SSI leads to less unfavorable fragility curves, while nonlinear soil response leads to smaller displacements and lower vulnerability. Most of these studies are based on nonlinear finite element analyses, and as such, carry along all their advantages and disadvantages. None of those studies, at least to our knowledge, proposes a simple yet straightforward methodology to include site amplification and soil-structure interaction effects in the seismic fragility assessment of buildings, especially when performing large-scale risk assessment.

To tackle this shortcoming, Petridis and Pitilakis (14; 15) developed a modular approach to include site amplification (SA) and/or SSI effects in the seismic fragility assessment of existing buildings. The focus is on existing structures, but the same approach could also be used to assess the effect of proper seismic design on reducing the vulnerability of new buildings. This paper builds on our previously published effort and extends our approach to buildings with a different lateral load-resisting system (MRF, dual frame-wall) and soil material type (sand, clay). We present a holistic method to include site amplification and soil-structure interaction effects on the fragility and vulnerability assessment of existing buildings typically found in the north Mediterranean cities. Moreover, in this paper we present two applications to further exploit the concept of the fragility modifiers (FM) as a simple and efficient solution to complement existing fragility curves with SA and/or SSI effects. Finally, in this study we propose an equation-based fragility modifier to ease the coding of SA and/or SSI effects into existing small- or large-scale risk assessment frameworks.

2. Methodology

A holistic methodology is developed to account for the effects of SSI and soil site amplification (SA) in fragility curves (16). This methodology aims toward a site-specific analysis but can be easily extended for application at risk assessment at the urban scale (15), combined with up-to-date seismic risk models (17). The basic steps of this modular approach are briefly described in this section.

The building model is created using finite element software in the first step. The spread footings of the building are modeled using the beam-on-nonlinear-Winkler foundation model (18) (BNWF). Next, the underlying soil profile is modeled to a depth whose response modifies the surface ground motion because of linear or nonlinear soil motion amplification. Then, a suite of ground motions is chosen for the analyses. In the case of actual recordings, these have to be recorded on bedrock (soil type A in all codes). Following, this bedrock ground motion is propagated to the free-field ground surface (or to the depth of the spread footings at free-field conditions) via any one-dimensional wave propagation software. This step is crucial for estimating the SA effects. In the light of the decoupled substructure approach to SSI (19), the free-field motion (FFM) is then modified to foundation input motion (FIM) using standard equations for kinematic interaction and foundation damping effects (for example, found in NIST2012 (4)). This foundation input motion is used to run a nonlinear dynamic analysis to calculate the building response. Finally, this building response is associated with appropriate drift- or strain-dependent damage states, based on its structural typology. The whole procedure is repeated for all selected bedrock ground motions, whereas bedrock ground motion scaling is performed in incremental dynamic analysis, i.e. scaling factors are applied at the bedrock level. Consequently, an ensemble of earthquake intensity-building response pairs is calculated. Fragility functions can then be calculated by estimating the probability of exceeding that predefined damage state. Vulnerability and loss curves can be calculated from the fragility curves.

Moreover, fragility modifiers (FM) are coefficients that modify any given readily available fragility curve for fixed-base structures, including SA and/or SSI effects. These FM are calculated based on the difference between the newly developed fragility curves and the traditional fixed-base ones. More details are provided in a subsequent section.

The step-wise procedure is detailed in (14), but some critical comments are elaborated below:

- The first step is to define the assessed building models. The seismic risk is a building-centric procedure in a building-specific or city-scale approach. Thus, the main prerequisite is the structural models' accurate and explicit definition and numerical simulation. The spread footings are modeled using beam-on-nonlinear-Winkler-foundation (18; 20) (BNWF) spring-type elements, attached at the foundation nodes of the structural models, to include inertial interaction effects (21). The BNWF element is generally used to approximate the nonlinear soil-foundation response in a substructure framework. Common engineering practice adopts elastic springs and – if possible – dashpots. Previous works (10; 14) show that nonlinear springs are a more elaborate and realistic approach than individual elastic springs and dashpots (22).

- The underlying soil profiles are independently modeled to capture the ground motion propagation from the bedrock to the free-field. The depth of the soil profile can affect the dynamic ground response. However, conforming with the recent design codes, the uppermost 30m of the soil can be explicitly modeled. A nonlinear finite element model analysis is required to derive the FFM. Again, in the context of this study, we found that (i) linear soil models tend to over-amplify ground motions at the surface and (ii) simplified pseudo-1D models, that is "Quad" 2D elements forming a soil column that behaves like an 1D element, can provide with the FFM within adequate accuracy. Research and commercial soil response software may also be used to derive the FFM.

- A set of recordings at bedrock (for example, recorded at soil type A according to EC8) is required to run the dynamic analyses. Selecting ground motions recorded on rock sites removes site and soil uncertainties, complying with explicit soil numerical models to capture the FFM. Besides, this selection is compatible with all current seismic hazard assessment methods. While this is the main prerequisite for ground motion selection, matching a uniform hazard spectrum is also advisable (23), to ensure that uniform probabilities of exceedance exist over the entire frequency range of interest . However, this filtering procedure is rather exhausting for the current recordings database, leaving no option for a cloud analysis using unscaled actual earthquake recordings. An incremental dynamic analysis (IDA) can be used to overcome this problem.

- Kinematic interaction effects transform the FFM to the FIM. Since the FFM is already derived, analytical equations (24; 4) can be used to generate the FIM, i.e., the input motion at the base of the spread footings of the building. Besides, the foundation damping further modifies the FIM from FFM. Foundation damping comprises soil hysteretic and radiation damping (4). Both are included in the beam-on-nonlinear-Winkler-foundation models.

- Incremental dynamic analysis (25) uses a relatively limited number of recordings incrementally scaled to account for different intensity levels, which corresponds well with the lack of plentiful recordings in the case of rock sites. IDA provides a cloud of intensity measure (IM) – engineering demand parameter (EDP) pairs to be post-processed for the fragility assessment. While there are a plethora of available methods for record selection for fragility assessment (the reader can find valuable information here (26; 27; 28; 29)), in our approach, IDA is performed by applying incrementally scaled ground motions at the base of the soil profiles (i.e., at the fictitious bedrock) to calculate the FFM. Then, each resulting FFM is transformed to FIM and applied at the base of the structural models to capture the corresponding building response.

- Finally, fragility curves can be calculated from the building response. Fragility curves represent the probability of exceeding a predefined limit state, as a function of an engineering demand parameter (EDP), under a seismic excitation of given intensity. Before the fragility assessment, an accurate definition of the damage states (DS) is required. This is often a subjective issue because various damage state definitions, drift-dependent or strain-dependent, regarding the selected EDP exist in literature. Then, fragility modifiers (FM) can be extracted from all fragility curves to appropriately modify existing curves to account for site amplification and soil-structure interaction effects. FM are especially valuable for a large-scale risk assessment.

Table 1
Indicative building properties

Seismic code	No/Low	Typical story height	3.0m
Concrete grade	B225	Span length (Low/Mid-rise)	4.0m
Longitudinal reinforcement grade	StIII	Span length (High-rise)	6.0m
Transverse reinforcement grade	StI	Typical beam size (Low/Mid-rise)	20/60cm
Transverse reinforcement spacing	Sparse	Typical beam size (High-rise)	25/70cm
Ground story height	4.5m	Typical column size	Varies w/ height
Low/mid-rise walls	20/400cm	High-rise walls	20/600cm

3. Fragility assessment of buildings

We perform a comprehensive fragility assessment for a broad set of existing RC buildings and soil profiles to evaluate (i) soil-structure interaction and (ii) soil site amplification effects on the corresponding fragility curves. At first, we calculate the fragility curves for buildings founded on bedrock. This *fixed-base-building-on-rock* case is the reference for all consequent analyses and comparisons. Then we calculate fragility curves for *fixed-base-buildings-on-soil* models. These configurations isolate the effects of (only) the soil site amplification on the fragility curves. Finally, the *flexible-base-building-on-soil* models are used to calculate the fragility curves, including SA and SSI effects. These different configurations aim to identify differences between the fragility curves for fixed-base-building-on-rock models and the SA and/or SSI -inclusive models in terms of the probability of exceeding a given damage state. We then produce fragility modifiers to accommodate for SA and/or SSI effects on any given fragility curve produced by a fixed-base-building-on-rock or fixed-base-building-on-soil concept. In this manner, we obtain an overview of the vulnerability related to different existing RC structures resting on various soil profiles.

The updated fragility curves are calculated for different building typologies and geometries, code provisions, foundation type, soil profile characteristics, and ground motions. Then, fragility modifiers are estimated as described in a subsequent section.

3.1. Building typology, geometry, and seismic code provision

A set of reinforced concrete buildings is sought, covering structures met in common engineering practice within the same typology. In particular, we follow the classification proposed by Kappos et al. (30) and the Global Earthquake Model (GEM) (31), selecting a 2-story (low-rise), a 4-story (mid-rise), and a 9-story (high-rise) building. Furthermore, for each building, we assume two different lateral load resisting systems, a moment-resisting frame, and a dual frame-wall system, each of which has three different configurations, notably bare, infilled, and pilotis (soft ground story). The buildings are designed and analyzed assuming low and moderate seismic code provisions. Such structures are commonly met in cities in southern Europe, built around the mid of the past century. The Table 1 shows indicative building properties.

We use OpenSees (32) to develop the corresponding numerical models using a fiber element approach. Distributed plasticity models allow yielding to occur at any location along the element. To implement them, we adopt the "forceBeamColumn" element object, which is based on the iterative force-based formulation, assuming five integration points along the length of the element.

The uniaxial "Concrete01" and "ReinforcingSteel" materials are selected to form the fiber sections for each structural element. "Concrete01" material object implements the modified Kent and Park concrete model (33) proposed by Scott et al. (34) with degraded linear unloading/reloading stiffness based on the work of Karsan and Jirsa (35). "ReinforcingSteel" implements the reinforcing steel material model, based on the backbone curve described by Chang and Mander (36).

3.2. Foundation type and modeling

Typical RC buildings found in Southern European cities were mainly built around the middle of the past century. Such structures typically rest on spread footings without interconnecting beams at the foundation. Inertial interaction effects (37) are modeled using the BNWF model. In particular, the "ShallowFoundationGen" command in OpenSees creates the BNWF model, i.e., a set of closely-spaced independent nonlinear springs, coupled with a dashpot and gap elements, calibrated against centrifuge experiments (38). Vertical springs distributed along the footing base aim to capture rocking, uplift, and settlement. In contrast, horizontal springs attached to the sides of the footing are used to capture the resistance against swaying and passive pressure. In all cases, the fixed-base models are used as a reference, representing the previous practice.

Furthermore, kinematic interaction effects are accounted for (39; 24), modifying the FFM to FIM. Kinematic interaction effects in our study are implemented assuming 2.0m of foundation depth.

3.3. Soil profile modeling

We select a set of seven single-layer soil profiles, parameterized mainly according to the soil shear wave velocity, while other soil characteristics are modified appropriately. Even though the soil depth might influence the soil response, we modeled the uppermost 30m of soil to conform with recent code provisions. While soils were categorized based on their shear wave velocity, analyses were run for sands and clays. The Table 2 presents the soil parameters that we considered for clay and sand and the chosen soil types according to Eurocode 8 (40).

Regarding the corresponding numerical models, a pseudo-1D approach is adopted, modeling the physical free-field as a soil column of two-dimensional "Quad" elements. Using OpenSees, a single "zeroLength" element is placed at the base of the soil column to define the dashpot (41). Soil nonlinearities are inherently included using the "PressureIndependMultiYield" and "PressureDependMultiYield" for clayey and sandy soil material, respectively. The input motion at the base of the soil model is defined in velocity terms. At the same time, the resulting force history

Table 2
Suggested soil parameter values used in OpenSees (32). Chosen soil types according to EC8.

Parameters	Clay			Sand		
	Soft	**Medium**	**Stiff**	**Loose**	**Medium**	**Med-dense**
Soil mass density [Mg/m^3]	1.3	1.5	1.8	1.7	1.9	2.0
Low-strain shear modulus [kPa]	1.3x10^4	6.0x10^4	1.5x10^5	5.5x10^4	7.5x10^4	1.0x10^5
Bulk modulus [kPa]	6.5x10^4	3.0x10^5	7.5x10^5	1.5x10^5	2.0x10^5	3.0x10^5
Cohesion [kPa]	18.0	37.0	75.0	-	-	-
Shear strain at max shear	0.1	0.1	0.1	0.1	0.1	0.1
Friction angle [deg]	0.0	0.0	0.0	29.0	33.0	37.0
Vs [m/s]	150/180	250/300/360	360/450	150/180	250/300/360	360/450
Type (EC8)	D	C	B	D	C	B

is obtained by multiplying the known velocity time series by a constant factor set as the product of the area of the soil column base with the mass density and the shear wave velocity of the underlying bedrock. The mesh dimensions are determined automatically, ensuring at the same time that an adequate number of elements fit within the wavelength of the shear waves considered. This guarantees that the mesh is refined enough to capture all the desired aspects of the propagating waves within the dynamic analyses.

3.4. Ground motions

For the for the fragility assessment, we selected a set of 11 actual earthquake recordings for the incremental dynamic analyses to follow, all of them recorded on sites classified as rock according to EC8 (40). This way, any site effects, and soil uncertainties are avoided, whereas any duplicate events are excluded to derive a set of independent records. Each event is considered only once, even excluding recordings of the same event at different stations and one of the perpendicular components of the recording. This aims to avoid double-accounting for the characteristics of a single event, in particular the frequency content. All the seismic events are characterized by a Mw > 5.5. There is, of course, variability in the chosen record spectra, but their normalized mean spectrum nearly matches the Type 1-EC8 spectrum for soil type A and the ASCE7-16 rock site spectrum. Recently, more elaborate earthquake record selection methods have been proposed. However, they are not compatible with our approach to explicitly include the nonlinear soil amplification effects.

Applying all these criteria for the ground motion selection procedure eliminates many recordings. However, the remaining set is considered adequate (42; 43) for the fragility assessment. Table 3 shows in detail the selected ground motions and Figure 1 shows the corresponding response spectra.

Table 3
List of actual earthquake records

Date	Location	Database Code	R_{epi} (km)	M_w	PGA (m/s^2)	$V_{s,30}$ (m/s)	Fault Mechanism
16/09/1978	Tabas/Iran	ESMD_59	12.00	7.35	3.16	826.00	Oblique
15/04/1979	Montenegro/Montenegro	ISESD_223	21.00	6.90	1.77	1083.00	Thrust
09/09/1998	App.Lucano/Italy	ITACA_614	9.80	5.60	1.62	1024.00	Normal
16/01/1995	Kobe/Japan	NGA_1108	25.40	6.90	2.85	1043.00	Strike-Slip
28/06/1991	Sierra Madre/Mexico	NGA_1645	6.46	5.61	2.71	821.69	Reverse
18/10/1989	Loma Prieta/USA	NGA_3548	20.35	6.93	4.12	1070.34	Reverse-Oblique
10/01/1987	Whittier Narrows/USA	NGA_680	13.85	5.99	1.10	969.07	Reverse-Oblique
17/01/1994	Northridge/USA	NGA_994	25.42	6.69	2.84	1015.88	Reverse
17/08/1999	Izmit/Turkey	T-NSMP_1109	3.40	7.60	1.65	826.11	Strike-Slip
13/12/1990	East Sicily/Italy	ITACA_314	28.30	5.60	0.61	871.00	Strike-Slip
10/06/2000	Western Tottori/Japan	KIK-Net_3775	31.37	6.60	1.55	967.27	Strike-Slip

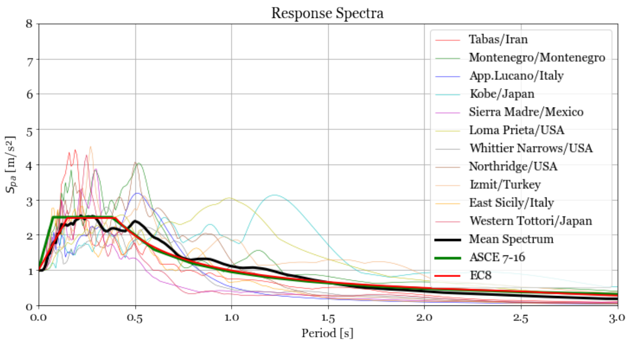

Figure 1: Response spectra for the selected ground motions, the mean response spectrum (in solid black line), and the EC8 / ASCE 7-16 response spectra for soil type A.

3.5. Dynamic analyses, building response and fragility curves

To obtain sets of intensity measure (IM) – engineering demand parameter (EDP) pairs, we conduct a series of incremental dynamic analyses. Even though spectral acceleration is recently considered as a superior IM to PGA, because it contains broader useful information of the ground motion, we selected PGA as IM because: (i) it is simple and applicable in large-scale analyses, in particular in the context of the European building stock typologies, and (ii) it allows running IDA analyses. In essence, here, IDA is performed in two separate stages: (i) to transfer the bedrock motions to the free-field, applying each ground motion at the base of the soil model, incrementally scaled from 0.0 to 1.0g. Selection of PGA as IM is critical at this stage. Then kinematic interaction equations are used to transform FFM into FIM. (ii) The second set of IDA is used to calculate the building response when applying each FIM at the base of the foundation numerical models, leading to a set of IM-EDP pairs.

The maximum interstory drift (maxISD) is selected as the EDP, calculated by the IDA. Nevertheless, maxISD was first chosen as EDP parallel to moment-curvature recordings that reflect structural damage. Such a comparison was

Table 4
Damage states definition

Damage	Index	Definition
Slight	SD	It usually corresponds to the limit of elastic behavior of the components
Moderate	MD	It usually corresponds to the peak lateral bearing capacity beyond which the structure loses some of its strength or deformation sets in at a constant rate of load
Extensive	ED	It usually corresponds to the maximum controlled deformation level for which a determined value of ductility is set. Up to this point, the structure can maintain its gravity load capacity
Complete	CD	Represents the attainment of Complete Damage (Collapse) level

deemed necessary, as maxISD is, in many cases, concentrated at the ground-level story, where foundation rotation due to SSI increases the interstory drift without causing additional structural damage (44). Petridis and Pitilakis (14) showed that (i) the maxISD follows the corresponding sectional curvature increase/decrease, and (ii) the foundation rotation contribution to drift is less than 10% of the total drift.

In general, maxISD is a convenient, user-friendly EDP and damage indicator that describes the global response of each building. Using drift-based damage state values (45; 46), slightly calibrated to approach the fragility curves published by Kappos et al. (30) for structures found in north Mediterranean cities, we describe the damage states (DS) as shown in Table 4 (43). One should note that the fragility curves proposed in Kappos et al. (30) are based on a hybrid approach, which combines statistical data with results from nonlinear dynamic or static analyses. Consequently, those curves include SA and SSI effects to a certain extent because of the statistical data part that includes various soil conditions.

Equation 1 describes the cumulative conditional probability of exceeding a DS for a given IM.

$$P[DS|IM] = \Phi(\frac{ln(IM) - ln(\overline{IM})}{\beta}) \quad (1)$$

where Φ is the standard normal cumulative distribution function, IM is the intensity measure of the earthquake, $\overline{IM}$ is the corresponding median value, β is the log-standard deviation, and DS is the damage state. In detail, the log-standard deviation parameter characterizes the total dispersion related to each fragility curve. Three primary sources of uncertainty which contribute to the total variability of any given limit state (NIBS 2004 (47)) are considered, namely (i) the variability related to the definition of the limit state value, (ii) the capacity of each structural model, and (iii) the seismic demand. The log-standard deviation referring to the definition of the limit states (47) is equal to 0.40. In contrast, the corresponding value regarding the capacity is assumed to be equal to 0.30 for no/low seismic code structural systems (47). The last source of uncertainty, associated with the seismic demand, is explicitly evaluated, estimating the dispersion for the logarithms of PGA – maxISD pairs, with respect to the used regression method.

4. Results

This section presents and discusses fragility curves for RC buildings, derived following our holistic methodology to account for local nonlinear site amplification and soil-structure interaction effects in a modular way. This section focuses on the difference between the derived fragility curves rather than providing a vast, indistinguishable set of fragility curves for each case.

Different soil shear wave velocities cause other site amplification effects and eventually have different foundation soil flexibility. Softer soil profiles generally trigger more significant site amplification effects (48) and foundation flexibility (22). Thus, one should expect that the influence of V_S is most pronounced for softer soil profiles.

In Figure 2 we plot the fragility curves for a 2-story MRF, regularly infilled building, resting on soil with soil shear wave velocity 250m/s (Figure 2 left) and 360m/s (Figure 2 right), and built with low seismic code provisions. The fragility curves are shown for the four damage states described in a previous section, ranging from slight damage to complete damage. The same color pattern for the damage states is retained throughout the paper. The dotted line is the reference curve for each case, i.e., the fragility curve corresponding to the specific damage state, referring to the particular fixed-base-building-on-rock (FBR). The solid lines are the fragility curves for the fixed-base building resting on the soil profile (and not on bedrock), i.e., including only site amplification (SA) effects. Finally, dashed lines are the fragility curves for the flexible-base-building-on-soil, i.e., including SA and SSI effects. In Figure 2 we see that for the softer soil profile ($V_{S,30} = 250m/s$, Figure 2 left), the fragility curves shift to the left (with respect to the reference FBR curves) when including SA effects, while they shift further to the left when including SA+SSI effects. In any case, a leftward shift of the fragility curves implies a fragility increase. For the specific 2-story MRF regularly infilled building, SSI effects are not significant when it is founded on soil with $V_{S,30} = 360m/s$ (see Figure 2 right).

Site amplification and SSI effects combined lead to a roughly 15-30% shift from the reference curve for the fixed-base-building-on-rock model for the particular case of the softer soil profile ($V_{S,30} = 250m/s$, Figure 2 left). On the contrary, insignificant or slight changes are observed for stiffer soil profiles, with SSI practically absent for $V_{S,30}$ values greater than 360m/s.

Figure 3 shows fragility curves for a 4-story MRF, regularly infilled building, resting on a soil profile with shear wave velocity 180m/s (Figure 3 left) and 300m/s (Figure 3 right), and built with low seismic code provisions. Our results show that SA tends to increase the fragility of the buildings from the reference case of the fixed-base-building-on-rock (FBR) case. Therefore, for the sake of clarity, only the effects of SA only and SA+SSI are highlighted in Figure 3. Because of SSI, fragility curves in Figure 3 are shifted to the left, implying fragility increase. This fragility increase

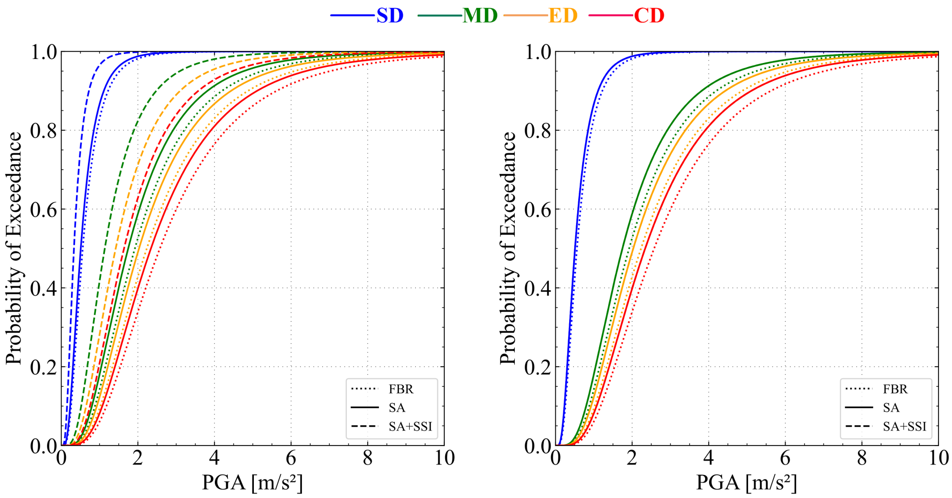

Figure 2: Fragility curves for a 2-story, MRF, regularly infilled building, resting on soil with $V_{S,30}$=**250m/s** (left) and $V_{S,30}$=**360m/s** (right). Solid-line fragility curves include site amplification (SA) effects only; dashed-line fragility curves include SA and SSI (SA+SSI) effects; dotted-line fragility curves are the reference curves for the fixed-base-building-on-rock (FBR) case. All curves are shown for the four damages states (SD, MD, ED, CD), ranging from slight to complete damage.

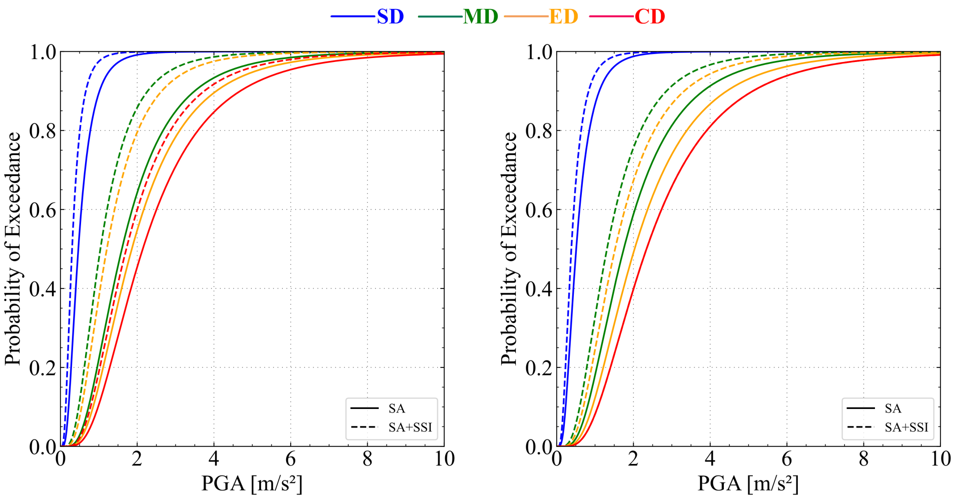

Figure 3: Fragility curves for a 4-story, MRF, regularly infilled building, resting on soil with $V_{S,30}$=**180m/s** (left) and $V_{S,30}$=**300m/s** (right). Solid-line fragility curves include site amplification (SA) effects only; dashed-line fragility curves include SA and SSI (SA+SSI) effects. All curves are shown for the four damages states (SD, MD, ED, CD), for slight to complete damage.

differs for different soil shear wave velocities and damage states and is more significant for lower soil V_S and lower DS.

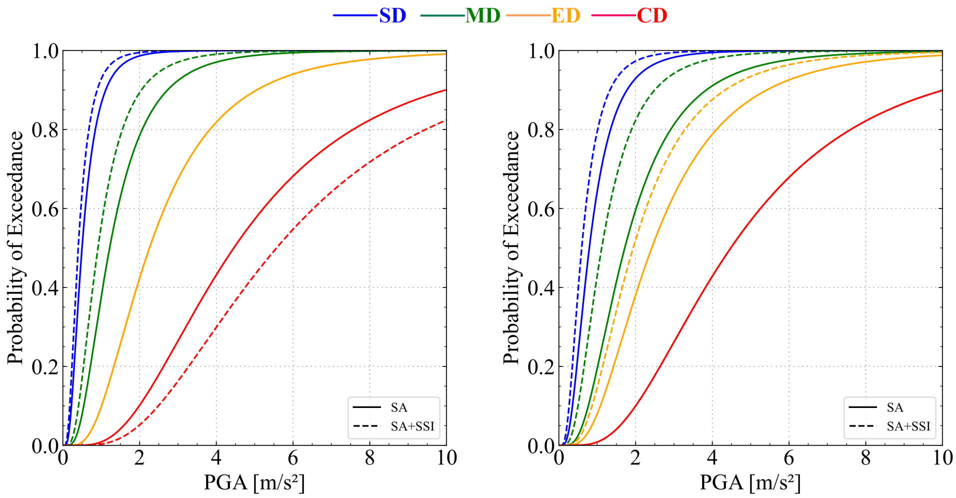

Figure 4: Fragility curves for the 9-story, MRF, **bare** (left), and **regularly infilled** (right) structure, resting on soil with $V_{S,30}$=180m/s. Solid-line fragility curves include only site amplification (SA) effects; dashed-line fragility curves include SA and SSI (SA+SSI) effects. All curves are shown for the four damages states (SD, MD, ED, CD), for slight to complete damage.

SSI effects alone increase the fragility up to 25% when comparing the median PGA between the SA and the SA+SSI cases in Figure 3. For higher DS, this ratio is usually lower (Figure 3 left) or even negligible for stiffer soil profiles (Figure 3 right). It is noted here that higher (more severe) DS mainly govern the vulnerability product.

From all our results, it is seen that softer soil profiles lead to additional structural damage, i.e., to a greater probability of exceeding a DS. This damaging effect becomes evident for V_S lower than approximately 360m/s, while the complete damage state is substantially affected by even softer soil profiles (V_S values lower than approximately 300m/s). If we were to set a threshold below which SA and SSI effects combined become significant for a seismic risk assessment procedure, a soil shear wave velocity V_S around 350m/s would be a reasonable limit.

However, the effect of SSI on fragility curves is not always detrimental. As seen in Figure 4 (left), for the 9-story moment-resisting bare frame building, SSI affects the fragility curves differently, depending on the DS. For lower DS, its effect on fragility is detrimental, whereas, for higher DS, it is beneficial. SA and SSI seem to affect the probability of exceeding different damage states differently. Limit values define DS, drift-dependent in this particular study, that roughly indicate whether an individual point from the IDA passes or not a specific DS. The lower the DS, the more sensitive it becomes to slight changes regarding the analyses outcome. Due to SA and/or SSI, even a slightly increased IDA maximum drift point might lead to the exceedance of a given low DS.

Besides, the presence of the infills seems to increase the fragility of the high-rise building, comparing Figures 4 (left) and 4 (right). Infills affect the structural response until they are disconnected from the RC frame during an

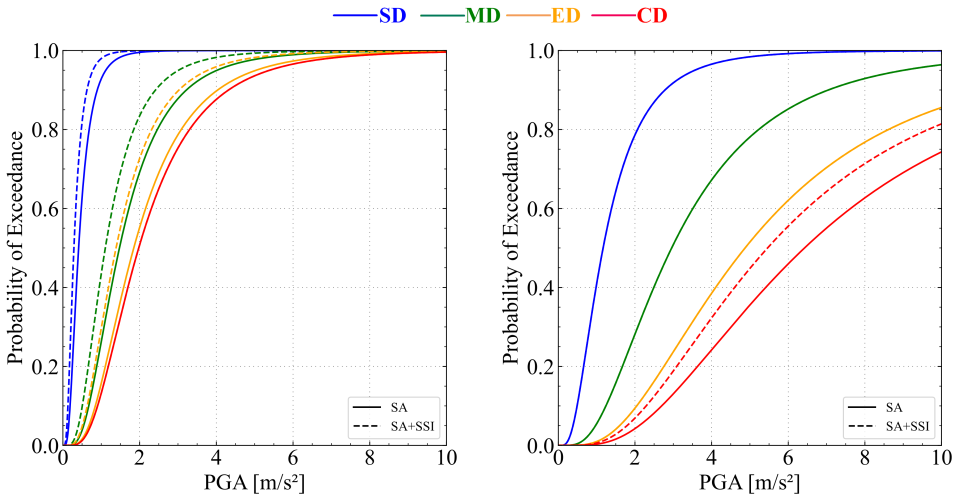

Figure 5: Fragility curves for a 4-story, **MRF** (left) and **dual frame-wall** (right), bare building, resting on soil with $V_{S,30}$=250m/s. Solid-line fragility curves include only site amplification (SA) effects; dashed-line fragility curves include SA and SSI (SA+SSI) effects. All curves are shown for the four damages states (SD, MD, ED, CD) for slight to complete damage.

earthquake. Because infills provide an extra layer of structural stiffness, they increase the SSI influence as the structure-to-soil stiffness ratio increases (4). Furthermore, infills are related to nonstructural damage. Although not discussed here, SSI effects often lead to increased structural displacements, injuring specific nonstructural elements, among which infills.

In addition, infills seem to increase more the fragility of the mid-rise (4-story) building (Figure 3 (left)), rather than the high-rise (9-story) building in Figure 4 (right), for all damage states. Finally, including SSI in the analysis leads to a rightward shift of the fragility curve for the complete damage (CD) state of the bare high-rise building (Figure 4 (left)), as opposed to the response of the 9-story regularly infilled structure in Figure 4 (right).

Figure 5 shows the fragility curves for a 4-story bare MRF building (left) and a bare dual frame-wall system building (right), resting on soil with shear wave velocity equal to 250m/s. The dual system building is significantly less vulnerable than the MRF because its structural system includes shear walls. Fragility curves for the MRF building (Figure 5 left) are affected (more or less) by SSI effects. In contrast, the dual building (Figure 5 right) remains practically unaffected, except for the complete damage state, which accounts for most of the loss estimation. Regarding the fragility curves shown in Figure 5, SSI shifts the fragility curves up to 20% with respect to the SA-only case.

However, this is not always the case. The damage transfer effect is the damage transfer from the shear wall to the frame parts of a dual building, triggered by foundation flexibility, rotation, and especially the absence of interconnecting beams between the footings. This damage transfer significantly affected the fragility of dual frame-wall

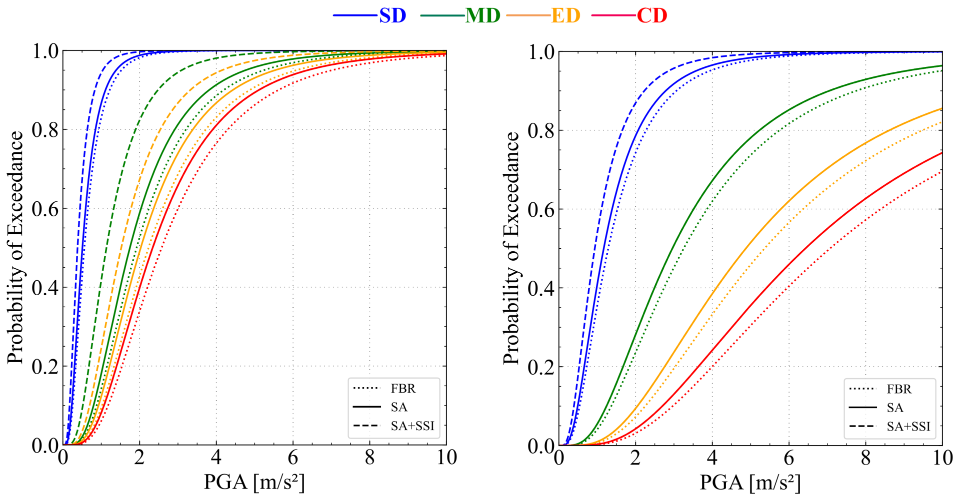

Figure 6: Fragility curves for a 4-story, **MRF** (left) and **dual** (right), regularly infilled building, resting on soil with $V_{S,30}$=250m/s. Solid-line fragility curves include site amplification (SA) effects only; dashed-line fragility curves include SA and SSI (SA+SSI) effects; dotted-line fragility curves are the reference curves for the fixed-base-building-on-rock (FBR) case. All curves are shown for the four damages states (SD, MD, ED, CD), ranging from slight to complete damage.

system buildings (14), leading to more significant additional losses. In such cases, SSI acts detrimentally and becomes apparent in the seismic fragility. MRF buildings, on the other hand, practically ignore this effect.

Figure 6 plots the fragility curves for a 4-story MRF regularly infilled building (left) and a dual frame-wall regularly infilled building (right), resting on soil with shear wave velocity equal to 250m/s. The dual system building is significantly less vulnerable than the MRF, mainly because its lateral load-resisting system includes shear walls. Site amplification (SA) effects are equally apparent for both structural systems (MRF and dual), i.e., the leftward shifting from the dotted curves of the fixed-base-building-on-rock (FBR) model is almost the same for all DS for both cases. In addition, SSI increases the fragility of the MRF building (Figure 6 left), whereas it does not affect the dual system building (Figure 6 right), except for the slight damage state. Interestingly, SSI effects on the fragility are more significant for the regularly infilled structure in Figure 6 (left) than the bare building in Figure 5 (left).

Furthermore, infills primarily affect MRF buildings, and their influence becomes negligible for dual systems (30). Following this remark, a similar impact is observed in fragility terms. However, it is less significant than other parameters (e.g., soil V_S). Infills provide an extra layer of structural stiffness and increase the SSI influence because the structure-to-soil stiffness ratio increases (21). On the other hand, the foundation flexibility increases the rotation and displacement of the structural elements (49), leading to more nonstructural damage and eliminating the contribution of infills to lateral stiffness.

Otherwise, the soil material does not seem to affect the fragility of the buildings. As seen in Figure 7, the fragility curves for a 2-story MRF bare building resting on clayey or sandy soil material (7 left and right, respectively) are

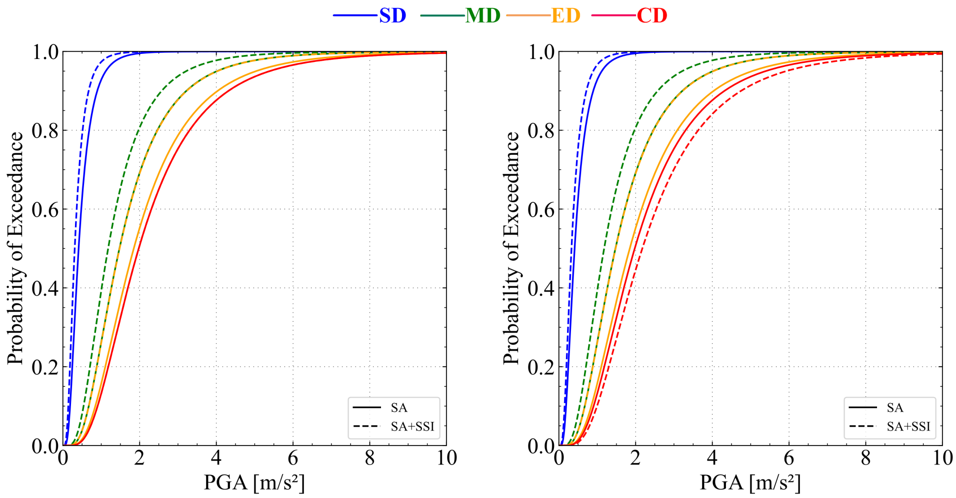

Figure 7: Fragility curves for a 2-story, MRF, bare building, resting on **clay** (left) and **sand** (right) soil with $V_{S,30}$=250m/s. Solid-line fragility curves only include site amplification (SA) effects; dashed-line fragility curves include SA and SSI (SA+SSI) effects. All curves are shown for the four damages states (SD, MD, ED, CD), ranging from slight to complete damage.

almost identical for all damage states, except for the complete damage state for sand where the effects of SA and SSI become beneficial. From our analyses and without accounting for soil depth variations in our approach, it seems safe to assume that any influence of the soil material on the fragility curves of a building should be attributed to its dynamic characteristics (for example, V_S) rather than on the material itself.

5. Practical uses for large-scale risk assessment

5.1. Fragility modifiers

Fragility modifiers (FM) provide an efficient and straightforward approach to include site amplification and soil-structure interaction effects in seismic risk assessment procedures (14). We used results from analyses of a set of 18 building typologies, 14 soil profiles, and 3 soil-foundation conditions to derive the corresponding sets of fragility and vulnerability curves. We employ the PGA corresponding to 50% probability of exceeding each DS (median PGA), and we estimate FM as the ratio between:

- *flexible-base-building-on-soil* and *fixed-base-building-on-rock* models, to include (local nonlinear) SA and SSI effects (Equation 2)

$$FM_{SA+SSI,i} = \frac{PGA_{50\%,flexible-base-on-soil,i}}{PGA_{50\%,fixed-base-on-rock,i}} \tag{2}$$

- *flexible-base-building-on-soil* and *fixed-base-building-on-soil* models, to isolate SSI effects (Equation 3)

$$FM_{SSI,i} = \frac{PGA_{50\%,flexible-base-on-soil,i}}{PGA_{50\%,fixed-base-on-soil,i}} \tag{3}$$

In Equations 2 and 3, i loops over Slight Damage (SD), Moderate Damage (MD), Extensive Damage (ED), and Complete Damage (CD) states. Ratios less than 1.00 indicate an increase in fragility (i.e., detrimental effects), and ratios greater than 1.00 imply a decrease in fragility (i.e., favorable influence).

Besides, Figure 8 shows a heat map of the FM_{SA+SSI} (Equation 2), including SA and SSI effects, for different lateral load-resisting systems, building height, infill conditions, damage states, soil materials, and local soil shear wave velocity below the building. The FM_{SA+SSI} are rounded appropriately for practical use (to the second decimal place). The darker the color on the heat map in Figure 8, the more significant the fragility increase because of SA and SSI is. These FM can be used to further modify fragility curves for existing (fixed-base-building-on-rock) RC buildings to include site amplification and soil-structure interaction effects. Engineering judgment can provide the engineer with a more specific value within each range.

On the other hand, Table 5 presents the FM_{SSI} for the SSI effects only, rounded appropriately for practical use, following the same pattern as the case discussed above. The tabular discretization is based on the structural type (MRF, dual system) and height (low, medium, high), the infill type (no/bare, regular, pilotis), the damage state (slight, moderate, extensive, complete), the soil material (clay or sand) and the shear wave velocity $V_{S,30}$ below the building. Values around 1.00 imply no/negligible influence of SSI, values lower than 1.00 suggest increased vulnerability due to SSI, and values greater than 1.00 correspond to favorable SSI effects. These table-based FM can be used, for example, to enhance literature fragility curves for fixed-base RC buildings with SSI effects, depending on their soil-foundation-structure configuration.

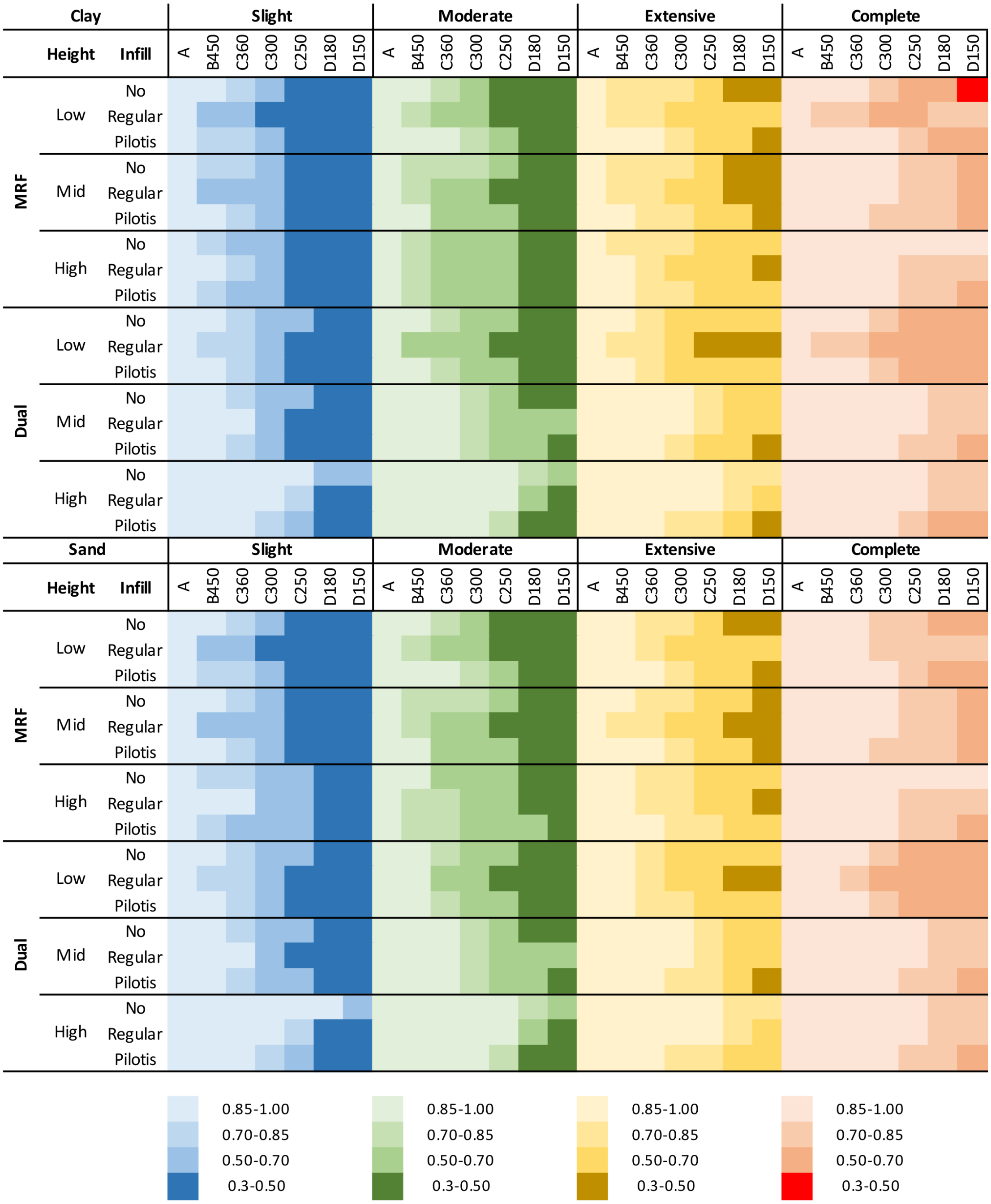

Figure 8: Heat map of the fragility modifiers (FM): Ratios between the *flexible-base-building-on-soil* and *fixed-base-building-on-rock* fragility curves. Darker colors imply a more significant fragility increase because of the combined SA and SSI

Table 5
flexible-base-building-on-soil over *fixed-base-building-on-soil* ratios of median PGA to exceed each DS (Equation 3), to isolate SSI effects.

Soil	System	Storeys	Infill	Slight					Moderate					Extensive					Complete				
				Damage – Soil shear wave velocity (Vs) and EC8 soil type																			
				360	C300	C250	D180	D150	360	C300	C250	D180	D150	360	C300	C250	D180	D150	360	C300	C250	D180	D150
Clay	MRF	2	No	1.00	1.00	0.75	0.70	0.70	1.00	1.00	0.80	0.75	0.70	1.00	1.00	0.80	0.75	0.70	1.00	1.00	1.00	0.80	0.70
		2	Regular	1.00	0.75	0.65	0.65	0.70	1.00	0.75	0.65	0.65	0.75	1.00	0.75	0.70	0.80	0.80	1.00	0.75	0.70	0.85	0.85
		2	Pilotis	1.00	1.00	0.70	0.70	0.65	1.00	1.00	0.75	0.70	0.70	1.00	1.00	0.80	0.75	0.75	1.00	1.00	1.00	0.80	0.80
		4	No	1.00	1.00	0.70	0.70	0.65	1.00	1.00	0.75	0.70	0.65	1.00	1.00	0.75	0.70	0.70	1.00	1.00	1.00	1.00	1.00
		4	Regular	1.00	0.75	0.75	0.65	0.70	1.00	0.75	0.65	0.65	0.70	1.00	0.75	0.75	0.65	0.70	1.00	1.00	1.00	0.80	1.00
		4	Pilotis	1.00	0.80	0.80	0.65	0.65	1.00	1.00	0.75	0.65	0.65	1.00	1.00	0.80	0.80	0.70	1.00	1.00	1.00	1.00	1.00
		9	No	1.00	1.00	0.70	0.80	0.80	1.00	0.75	0.75	0.75	0.75	1.00	0.85	0.80	1.00	1.00	1.00	1.25	1.25	1.25	1.25
		9	Regular	1.00	0.80	0.75	0.75	0.65	1.00	0.70	0.80	0.65	0.55	1.00	0.80	0.80	0.80	0.75	1.00	1.00	1.00	1.00	1.00
		9	Pilotis	1.00	0.75	0.75	0.75	0.65	1.00	1.00	0.75	0.75	0.65	1.00	1.00	1.00	0.85	0.80	1.00	1.00	1.00	1.00	1.00
	Dual	2	No	1.00	0.80	0.70	0.70	0.65	1.00	0.85	0.85	0.65	0.65	1.00	0.75	0.70	0.75	0.75	1.00	0.80	0.80	0.80	0.80
		2	Regular	1.00	0.80	0.70	0.65	0.65	1.00	1.00	0.80	0.70	0.65	1.00	0.80	0.70	0.75	0.75	1.00	0.80	0.75	0.75	0.75
		2	Pilotis	1.00	1.00	0.70	0.70	0.65	1.00	1.00	1.00	0.70	0.70	1.00	0.70	0.70	0.70	0.75	1.00	1.00	0.80	0.70	0.70
		4	No	1.00	1.00	1.00	0.70	0.65	1.00	1.00	1.00	0.75	0.70	1.00	1.00	1.00	0.75	0.65	1.00	1.00	0.85	0.80	0.80
		4	Regular	1.00	1.00	0.80	0.65	0.65	1.00	1.00	1.00	0.75	0.70	1.00	1.00	1.00	0.80	0.75	1.00	1.00	1.00	0.80	0.80
		4	Pilotis	1.00	1.00	0.75	0.65	0.60	1.00	1.00	1.00	0.75	0.70	1.00	1.00	0.80	0.70	0.65	1.00	1.00	0.85	0.80	0.75
		9	No	1.00	1.25	1.25	1.25	1.25	1.00	1.00	1.20	1.20	1.20	1.00	1.00	1.00	1.00	1.00	1.00	1.00	1.00	1.00	1.00
		9	Regular	1.00	1.00	1.00	1.00	0.80	1.00	1.00	1.00	1.00	0.75	1.00	1.00	1.00	0.85	0.75	1.00	1.00	1.00	0.85	0.75
		9	Pilotis	1.00	1.00	1.00	1.00	0.85	1.00	1.00	1.00	1.00	0.70	1.00	1.00	1.00	0.85	0.70	1.00	1.00	1.00	1.00	0.80
Sand	MRF	2	No	1.00	1.00	0.80	0.70	0.70	1.00	1.00	0.80	0.75	0.70	1.00	1.00	0.80	0.75	0.70	1.00	1.00	1.00	0.85	0.80
		2	Regular	1.00	0.85	0.75	0.65	0.70	1.00	0.75	0.65	0.65	0.75	1.00	0.75	0.75	0.80	0.80	1.00	1.00	0.85	0.85	0.85
		2	Pilotis	1.00	1.00	0.75	0.70	0.70	1.00	1.00	0.75	0.70	0.70	1.00	1.00	0.80	0.75	0.75	1.00	1.00	1.00	0.85	0.85
		4	No	1.00	1.00	0.75	0.70	0.70	1.00	1.00	0.75	0.70	0.65	1.00	1.00	0.75	0.70	0.70	1.00	1.00	1.00	1.00	1.00
		4	Regular	1.00	0.85	0.75	0.65	0.70	1.00	0.75	0.65	0.65	0.70	1.00	0.75	0.75	0.70	0.70	1.00	1.00	1.00	0.85	1.00
		4	Pilotis	1.00	0.85	0.80	0.65	0.70	1.00	1.00	0.75	0.65	0.65	1.00	1.00	0.80	0.80	0.70	1.00	1.00	1.00	1.00	1.00
		9	No	1.00	1.00	0.75	0.80	0.80	1.00	0.75	0.75	0.75	0.75	1.00	0.85	0.80	1.00	1.00	1.00	1.25	1.25	1.25	1.25
		9	Regular	1.00	0.85	0.75	0.75	0.70	1.00	0.70	0.80	0.65	0.55	1.00	0.80	0.80	0.80	0.75	1.00	1.00	1.00	1.00	1.00
		9	Pilotis	1.00	0.85	0.80	0.75	0.70	1.00	1.00	0.75	0.75	0.65	1.00	1.00	1.00	0.85	0.80	1.00	1.00	1.00	1.00	1.00
	Dual	2	No	1.00	0.85	0.70	0.70	0.65	1.00	0.85	0.85	0.65	0.65	1.00	0.75	0.70	0.70	0.70	1.00	0.85	0.80	0.80	0.80
		2	Regular	1.00	0.85	0.70	0.70	0.65	1.00	1.00	0.80	0.70	0.65	1.00	0.80	0.70	0.75	0.70	1.00	0.85	0.80	0.75	0.75
		2	Pilotis	1.00	1.00	0.75	0.70	0.65	1.00	1.00	1.00	0.70	0.70	1.00	0.70	0.70	0.70	0.70	1.00	1.00	0.85	0.75	0.75
		4	No	1.00	1.00	1.00	0.70	0.70	1.00	1.00	1.00	0.75	0.70	1.00	1.00	0.80	0.75	0.65	1.00	1.00	0.85	0.80	0.80
		4	Regular	1.00	1.00	0.80	0.70	0.65	1.00	1.00	1.00	0.75	0.70	1.00	1.00	1.00	0.80	0.75	1.00	1.00	1.00	0.80	0.80
		4	Pilotis	1.00	1.00	0.75	0.70	0.70	1.00	1.00	1.00	0.75	0.70	1.00	1.00	0.80	0.70	0.65	1.00	1.00	1.00	0.80	0.75
		9	No	1.00	1.25	1.25	1.25	1.25	1.00	1.00	1.20	1.20	1.20	1.00	1.00	1.00	1.00	1.00	1.00	1.00	1.00	1.00	1.00
		9	Regular	1.00	1.00	1.00	1.00	0.80	1.00	1.00	1.00	1.00	0.75	1.00	1.00	0.85	0.85	0.75	1.00	1.00	1.00	0.85	0.80
		9	Pilotis	1.00	1.00	1.00	1.00	0.85	1.00	1.00	1.00	1.00	0.70	1.00	1.00	0.85	0.85	0.70	1.00	1.00	1.00	1.00	0.85

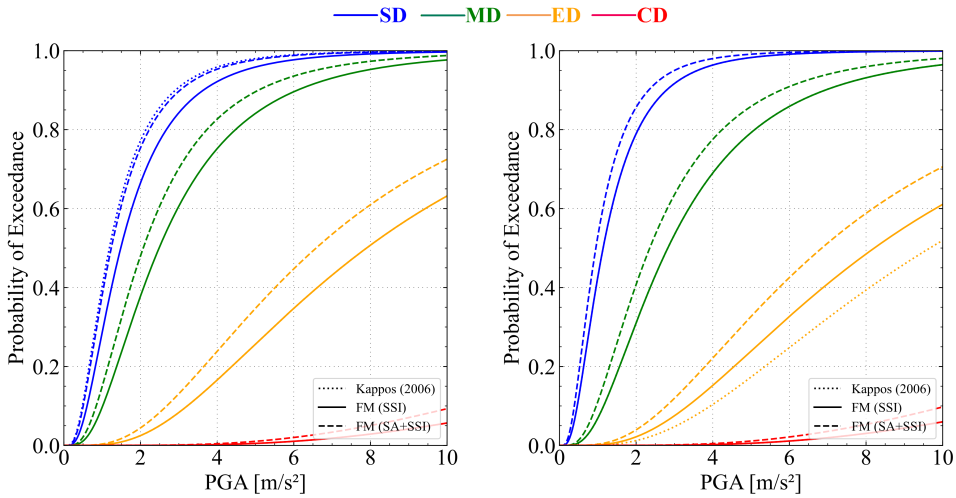

Figure 9: Fragility curves for a 9-story, dual, **bare** (left) and **pilotis system** (right) building, resting on soil with $V_{S,30}$=180m/s. Solid-line fragility curves include SSI effects only via the use of FM; dashed-line fragility curves include site amplification and SSI (SA+SSI) effects via the use of FM; dotted lines represent the reference curves derived from Kappos et al. (30). All curves are shown for the four damages states (SD, MD, ED, CD), ranging from slight to complete damage.

5.2. Application of FM

To demonstrate the applicability of the fragility modifiers, we use as an example the FM in Table 5 on existing fragility curves that typically ignore soil site amplification and SSI effects. In particular, using the proposed FM of Table 5, we modify a set of existing fragility curves to approach the ones that include SSI effects when site amplification effects are not explicitly addressed, Figure 8 provides an alternative, for FM to modify the existing fragility curves to embed site amplification and SSI effects.

5.2.1. Application example one

For example, we present the fragility curves for a 9-story dual frame-wall building resting on soft soil with $V_{S,30} = 180m/s$. In Figure 9, the fragility curves proposed by Kappos et al. (30) are used as reference. The FM in Figure 8 modify those reference curves to include site amplification and soil-structure interaction (SA+SSI) effects. On the contrary, the proposed FM in Table 5 can be used to alter the reference curves to have solely SSI effects. Since only mild SSI effects are apparent for the 9-story dual system building resting on soft soil with $V_{S,30} = 180m/s$, the FM value in Table 5 is around 1.00. Therefore, in case we include only SSI effects, the Kappos et al. fragility curves practically coincide with the FM(SSI) curves in most cases.

Additionally, for the particular extensive damage (ED) curve regarding the 9-story dual system building with pilotis (Figure 9, right), using Table 5 we obtain a FM equal to 0.85. That means that to explicitly include SSI effects only, we have to multiply the median PGA value of the reference curve of Kappos et al. by 0.85 to obtain the PGA that corresponds to 50% probability of exceeding the slight damage state. More specifically, we multiply $\text{PGA}_{50\%}$ =

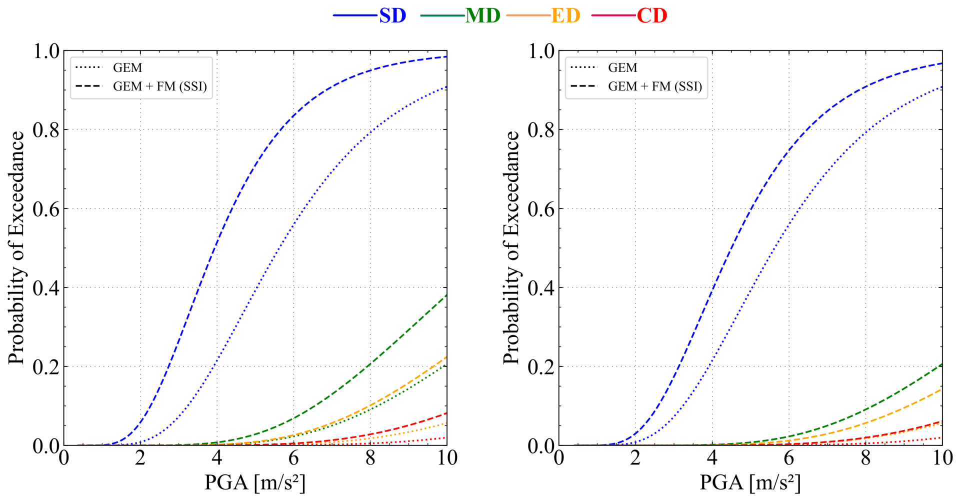

Figure 10: Fragility curves for a 2-story, dual frame-wall system, regularly infilled building, resting on soil with $V_{S,30}$=**250m/s** (left) and $V_{S,30}$=**300m/s** (right). Dashed-line fragility curves include SSI effects, calculated using the concept of FM. Dotted lines represent the fixed-base-building-on-rock reference curves, as given by GEM (31). All curves are shown for the four damages states (SD, MD, ED, CD), ranging from slight to complete damage.

9.60m/s^2 with FM = 0.85, which equals to PGA$_{50\%}$ = 8.16m/s^2 for the SSI-inclusive ED curve (FM(SSI)). Respectively, we can use the FM of Figure 8 to address both SA and SSI effects. This time, PGA$_{50\%}$ = 9.60m/s^2 is multiplied with a FM that ranges from 0.50 to 0.70 –using engineering judgment let us assume 0.70 for this example– which equals to PGA$_{50\%}$ = 6.72m/s^2 for the SA+SSI inclusive ED curve.

As mentioned, the fragility curves by Kappos et al. (2006) (30) curves are derived in a hybrid manner that implicitly includes a portion of SA and SSI effects because of the statistical earthquake data employed. From a general point of view, the engineer or risk analyst should be careful not to double-account for site amplification and/or SSI effects when the fragility curves used as reference are not explicitly derived from fixed-base models without the influence of site amplification. To practically overtake this pitfall, in the example above, we exerted engineering judgment and selected the FM equal to 0.70 out of a possible range from 0.50 to 0.70, minimizing additional site amplification influence.

5.2.2. Application example two

Conversely, FM derived from Table 5 alone can be used to modify, for example, the existing Global Earthquake Model (GEM) (31) fragility curves appropriately, to account only for SSI effects, as seen in Figure 10. In this manner, site amplification effects can be accounted for using any available seismic hazard model. In essence, fragility curves include SSI, while site amplification effects are considered via detailed site response analyses or using the available site amplification factors found in the literature. In the latter case, site amplification remains part of the hazard component, while SSI is embedded in the fragility counterpart.

In this example, to account only for SSI effects on the fragility curve for slight damage of a 2-story, regularly infilled dual system building resting on clay soil with $V_{S,30}$=250m/s (see Figure 10 left), using Table 5 we obtain a FM equal to 0.70. This means that we have to multiply the median PGA value of the slight damage curve of GEM by 0.70 to obtain the PGA that corresponds to 50% probability of exceeding the slight damage state. In particular, using the GEM SD curve of Figure 10 (left), we multiply $\text{PGA}_{50\%} = 5.71\text{m/s}^2$ with FM = 0.70, which equals to $\text{PGA}_{50\%} = 4.0\text{m/s}^2$ for the SSI-inclusive SD curve.

5.3. Equation form of FM

To help the risk analyst, the designer engineer, or any stakeholder to account for SSI effects in their risk calculations, we provide below an equation form of the fragility modifiers FM. Using the optimization scheme of the least-squares regression, we attempted to fit an equation in the data of Table 5. We did not fit an equation to our data including site amplification effects on fragility modifiers, because the error in the fitting was large enough to make the approach inapplicable. The selected optimization scheme can solve a nonlinear least-squares problem with bounds on the variables. Fitting may be achieved using various functions as a base. Here, our analyses' -noisy- output data, namely the FM values, cannot be accurately represented by simplified functions, such as a linear or a polynomial equation. Thus, fitting is achieved using the optimization scheme of the least-squares regression provided in SciPy that further permits nonlinear regression methods.

The resulting Equation 4 can be readily used to code FM into software applications rather than manually transfer table values. One can account for SSI effects on the traditional fragility curves for fixed-base structures. Nevertheless, such an approach is inevitably accompanied by a significant impact on the accuracy of the FM values.

$$\begin{aligned} FM_i = -0.027 \times LS^{-12.642} + 0.029 \times NS^{0.743} \\ +2.873 \times V_S^{0.059} - 3.19 \end{aligned} \tag{4}$$

where,

- LS: Lateral load-resisting system (takes value "1" for MRF and "2" for Dual system)
- NS: Number of stories (takes values 1 to 12)
- V_S: Shear wave velocity of underlying soil layer(s) (takes values 150m/s to 1000m/s). According to the literature (4; 50), the V_S can be estimated as the average shear wave velocity of a homogeneous soil layer beneath the foundation for SSI analyses. This soil layer should be of depth ranging from half the foundation width up to two times the foundation width for a more accurate representation of the foundation soil dynamic characteristics.

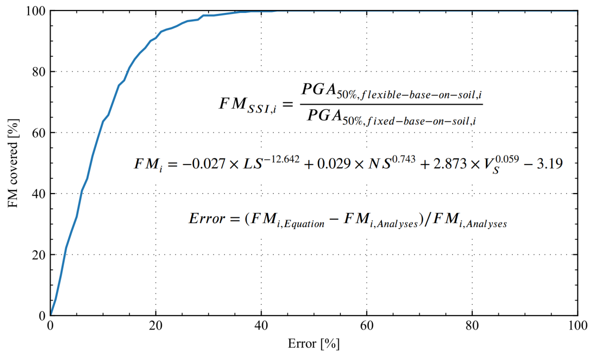

Figure 11: Error [%] versus FM covered [%].

During the optimization scheme of the least-squares regression method, we found that infills and soil type negligibly affect the outcome. Also, we avoided the refinement for different DS since it over-complicated the derived equation with additional variables without reaching a more accurate solution. On the other hand, Equation 4 is easily implemented in any application without the strict, compatible refinement of the typologies of the buildings and soils adopted in each study.

To evaluate the effectiveness of the proposed Equation, we estimated the percentage of the FM covered by Equation 4, with respect to the error percentage. Essentially, we compare the equation output with the FM derived analytically for all the cases included in this study. The error is defined in Equation 5.

$$Error = (FM_{i,Equation} - FM_{i,Analyses})/FM_{i,Analyses} \tag{5}$$

where i refers to the examined configuration (lateral load-resisting system, number of stoies, soil V_S), $FM_{i,Equation}$ is the FM value derived using Equation 4, and $FM_{i,Analyses}$ represents the FM derived from our dynamic analyses. Naturally, the larger the acceptable error, the higher the percentage of the FM adequately calculated using Equation 4 is, within this accepted error limit. This is further interpreted in Figure 11. For example, accepting a 20% error practically means that using the FM's equation form, one accurately covers 90% of the FM shown in Table 5.

In addition, to obtain an overview of the case-specific perspective of the effectiveness of Equation 4, we present in Figure 12 an error heat map of the equation-based approach. Based on the deviations observed in Figure 12 and the accepted level of error with respect to Figure 11, we concluded that using the table-based FM (in Figure 12) produces more accurate results and can be used when smaller groups of buildings are examined, e.g., single buildings or city blocks. On the contrary, equation-based FM (see Equation 4) values are helpful for large-scale (e.g., entire cities) applications, where software/coding approaches are utilized. Also, large-scale applications reduce the error observed

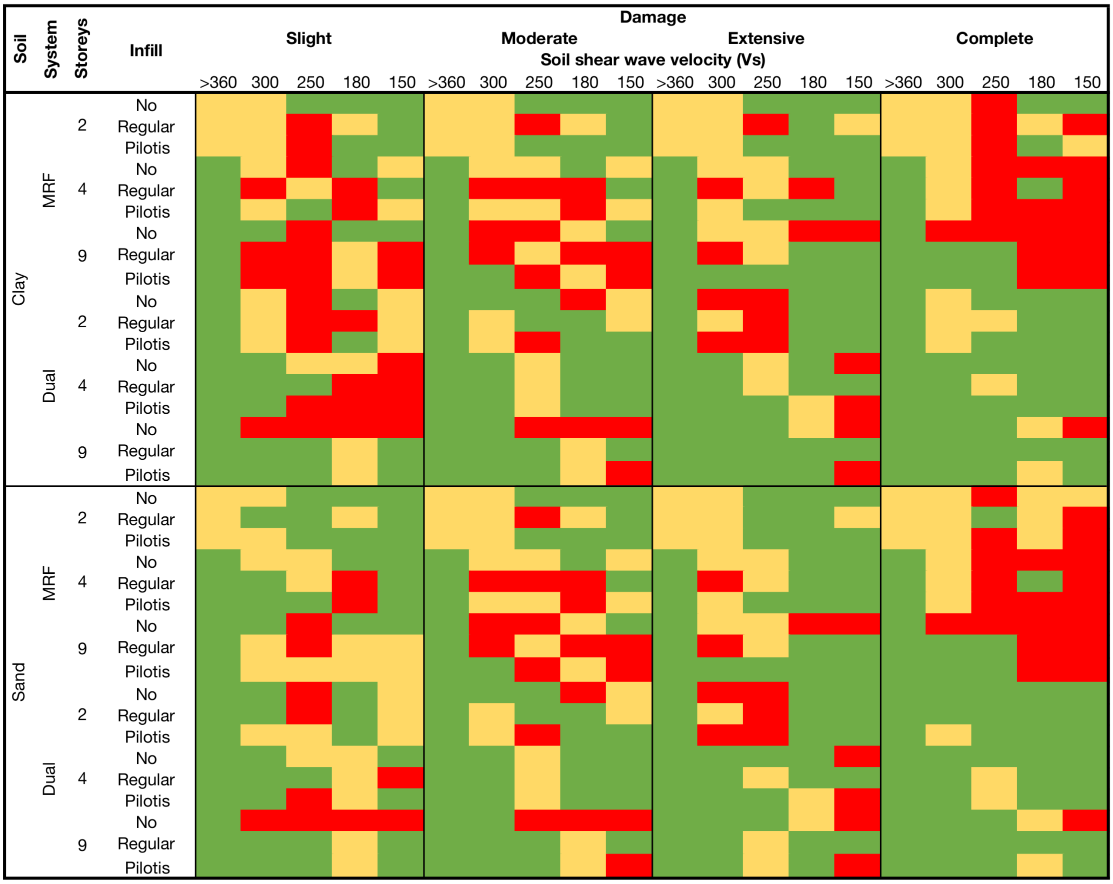

Figure 12: Error heat map for Equation 5. Green: 0-5%; Yellow: 5-10%; Red: >10% error.

due to the large number of buildings/soils included and the involvement of other parameters that more extensively influence the outcome.

6. Conclusions

This study investigates the effects of site amplification (SA) and soil-structure interaction (SSI) on the earthquake vulnerability of existing moment-resisting frame and dual system buildings in southern European cities. We found that SA and SSI significantly influence the building response. The methodology previously developed (14) to study the effects of SA and SSI on the fragility curves is further extended to buildings with a different lateral load-resisting system (MRF, dual frame-wall), height (low-rise, mid-rise, and high-rise), infill conditions (no/bare, regular, pilotis), soil shear wave velocity (150m/s to 450m/s) and soil material type (sand, clay). We propose a modular, holistic method to include SSI-only or SA+SSI effects in an earthquake vulnerability assessment, using fragility modifiers (FM). We also provide an easy-to-use equation form of the FM.

Our main conclusions are summarized below:

- The soil material (sand or clay) was found to have a minor role in the fragility and vulnerability of the building.
- On the other hand, the soil shear wave velocity below the foundation seems to be a leading contributor to the final fragility/vulnerability outcome, affecting both site amplification and SSI effects. A more detailed approach could include also site depth effects on the ground response. The effects of SA and/or SSI are minor for $V_S > 350m/s$.
- Four damage states were examined, showing that SA and SSI affect each fragility curve differently for each DS. In general, soil-related effects were more pronounced at lower DS.
- Damage transfer effect, that is, damage transfer from the shear wall to the frame parts of a dual frame-wall building, triggered by SSI, was found to affect fragility significantly. Consequently, in that case, SSI may modify the vulnerability of the building, leading to more significant additional losses. On the other hand, MRF buildings practically ignore this damage transfer effect. However, the structural response of MRF is also affected by SA and SSI effects.
- The building height and the presence of infill walls were found to differentiate the fragility curves. In particular, SSI triggered infill damage even for low PGA levels, which usually led to more significant losses in the long run.
- SSI effects, when present, lead up to a 25% differentiation between the fixed-base and flexible-base fragility curves.

Acknowledgments

We acknowledge support from the European project Seismology and Earthquake Engineering Research Infrastructure Alliance for Europe - SERA - H2020 (Grant Agreement 730900). We would like to thank Professor Andreas Kappos and Professor Anastasios Anastasiadis for the fruitful discussions and their comments during the course of our work.

A. Python application of the equation-based FM calculation

A code snippet example is given here to show a possible use case of Equation 4 in computational applications. This snippet defines Equation 4 as a function (named EFM). After that, the EFM function is called to modify a set of fragility curves by multiplying each median value with the FM estimated. Furthermore, the corresponding vulnerability curves are derived, adopting the Kappos et al. (30) damage index. The transformation of the fragility into vulnerability curves is implemented using the total probability relation. The damage probability is defined as the distance between two successive fragility curves for a given intensity, while this value is then multiplied by the corresponding damage index ratio.

As already mentioned,

- LS: Lateral load-resisting system (use "1" for MRF and "2" for Dual system)
- NS: Number of stories (takes values 1 to 12)
- V_S: Shear wave velocity of underlying soil layer(s) (takes values 150m/s to 1000m/s).

```
# LS: Lateral load-resisting system (1:MRF, 2:Dual)
# NS: Number of stories (1-12)
# VS: Shear wave velocity of underlying layer(s) (150-1000m/s)
# Python Dictionary format:
# Fragility[’Median’][Typology] = [Median for each Damage State]
# Fragility[’Stdv’][Typology] = [Standard deviation]

# Equation as function
def EFM(LS,NS,VS):
    EFMi = -0.027 * LS**(-12.642) + 0.029 * NS**(0.743) + 2.873 * VS**(0.059) - 3.19
    return EFMi

## Example: 4-story MRF, regularly infilled, low code
# Append literature fragility curves
# (medians and standard deviation)
Fragility[’Median’][’RD59_4s_mrf_rinf’] = [0.5594, 1.9214, 2.2320, 2.5743]
Fragility[’Stdv’][’RD59_4s_mrf_rinf’] = 1.8397
Model = ’RD59_4s_mrf_rinf’

# Call EMF to calculate equation-based FM for a MRF (i.e.,=1), 4-story (i.e.,=4)
```

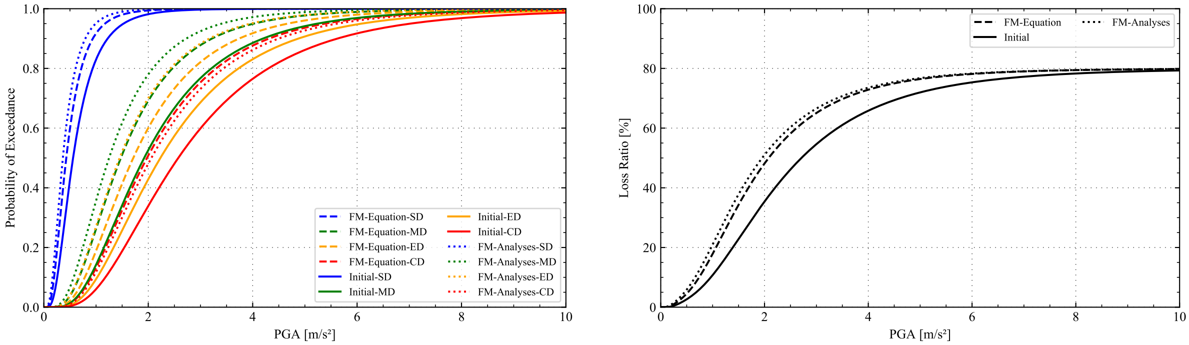

(a) (b)

Figure 13: Fragility curves (left) and vulnerability curves (right) for a 4-story MRF, regularly infilled, low-code building. FM-Equation denotes the fragility curves derived using the equation-based FM; FM-Analyses represents the fragility curves derived using the table-based FM (see Table 5); Initial corresponds to the reference curves used in this example.

```
# building on soil with Vs=180m/s (i.e,=180)
EFMi = EFM(1, 4, 180)

for i in range(0,4):
    Fragility['Modified_Median'][Model].append(EFMi * Fragility['Median'][Model][i])
    Stdv = Fragility['Stdv'][Model]

# Call functions to estimate/plot fragility and vulnerability

ModMedian = Fragility['Modified_Median'][Model]
FragCurve = FragPlot(ModMedian,Stdv,'-','Fragility')
VulnPlot(FragCurve,'-','Vulnerability')
```

Also, indicative plots of the outcome are presented in fragility (Figure 13 left) and vulnerability terms (Figure 13 right). Based on the derived vulnerability curves, good convergence of the table-based and the equation-based approaches is seen.

References

[1] D. D'Ayala, A. Meslem, D. Vamvatsikos, K. Porter, T. Rossetto, V. Silva, Guidelines for Analytical Vulnerability Assessment - Low/Mid-Rise, GEM Technical Report (2015) 162doi:10.13117/GEM.VULN-MOD.TR2014.12.

[2] V. Silva, S. Akkar, J. Baker, P. Bazzurro, J. M. Castro, H. Crowley, M. Dolsek, C. Galasso, S. Lagomarsino, R. Monteiro, D. Perrone, K. Pitilakis, D. Vamvatsikos, Current challenges and future trends in analytical fragility and vulnerability modelling, Earthquake Spectra 35 (4) (2019) 1927–1952.

URL https://doi.org/10.1193/042418EQS101O

[3] G. Mylonakis, G. Gazetas, Seismic Soil-Structure Interaction: Beneficial or Detrimental?, Journal of Earthquake Engineering 4 (3) (2000) 277–301. doi:10.1080/13632460009350372.
URL http://www.tandfonline.com/doi/abs/10.1080/13632460009350372

[4] NIST, Soil-Structure Interaction for Building Structures, Tech. rep. (2012).

[5] C. Bolisetti, A. S. Whittaker, J. L. Coleman, Linear and nonlinear soil-structure interaction analysis of buildings and safety-related nuclear structures, Soil Dynamics and Earthquake Engineering 107 (January 2016) (2018) 218–233. doi:10.1016/j.soildyn.2018.01.026.

[6] Y. Tang, J. Zhang, Probabilistic seismic demand analysis of a slender rc shear wall considering soil-structure interaction effects, Engineering Structures 33 (1) (2011) 218 – 229.

[7] E. Saez, F. Lopez-Caballero, A. Modaressi-Farahmand-Razavi, Effect of the inelastic dynamic soil-structure interaction on the seismic vulnerability assessment, Structural Safety 33 (1) (2011) 51–63.

[8] P. Rajeev, S. Tesfamariam, Seismic fragilities of non-ductile reinforced concrete frames with consideration of soil structure interaction, Soil Dynamics and Earthquake Engineering 40 (2012) 78–86. doi:10.1016/j.soildyn.2012.04.008.
URL http://dx.doi.org/10.1016/j.soildyn.2012.04.008

[9] F. Behnamfar, M. Banizadeh, Effects of soil-structure interaction on distribution of seismic vulnerability in RC structures, Soil Dynamics and Earthquake Engineering 80 (2016) 73–86.

[10] S. Karapetrou, S. Fotopoulou, K. Pitilakis, Seismic vulnerability assessment of high-rise non-ductile rc buildings considering soil structure interaction effects, Soil Dynamics and Earthquake Engineering 73 (2015) 42 – 57.

[11] K. Pitilakis, S. Karapetrou, S. Fotopoulou, Consideration of aging and SSI effects on seismic vulnerability assessment of RC buildings, Bulletin of Earthquake Engineering 12 (4) (2014) 1755–1776.

[12] S. Karafagka, S. Fotopoulou, D. Pitilakis, Fragility curves of non-ductile RC frame buildings on saturated soils including liquefaction effects and soil-structure interaction, Bulletin of Earthquake Engineering (mar 2021). doi:10.1007/s10518-021-01081-5.
URL http://link.springer.com/10.1007/s10518-021-01081-5

[13] F. Cavalieri, A. Correia, H. Crowley, R. Pinho, Dynamic soil-structure interaction models for fragility characterisation of buildings with shallow foundations, Soil Dynamics and Earthquake Engineering 132 (2020). doi:10.1016/j.soildyn.2019.106004.

[14] C. Petridis, D. Pitilakis, Fragility curve modifiers for reinforced concrete dual buildings, including nonlinear site effects and soil-structure interaction, Earthquake Spectra 36 (4) (2020) 1930–1951. doi:10.1177/8755293020919430.

[15] C. Petridis, D. Pitilakis, Large-scale seismic risk assessment integrating nonlinear soil behavior and soil-structure interaction effects, Bulletin of Earthquake Engineering (2021). doi:10.1007/s10518-021-01237-3.

[16] C. Petridis, Seismic risk assessment of reinforced concrete buildings including nonlinear soil structure interaction and site amplification effects, Ph.D. thesis, Aristotle University of Thessaloniki.

[17] E. Riga, A. Karatzetzou, S. Apostolaki, H. Crowley, K. Pitilakis, Verification of seismic risk models using observed damages from past earthquake events, Vol. 19, Springer Netherlands, 2021. doi:10.1007/s10518-020-01017-5.
URL https://doi.org/10.1007/s10518-020-01017-5

[18] C. Harden, T. Hutchinson, G. R. Martin, B. L. Kutter, Numerical Modeling of the Nonlinear Cyclic Response of Shallow Foundations, Tech. rep. (2005).

[19] A. S. Veletsos, J. Meek, Dynamic behaviour of building-foundation systems, Earthquake Engineering and Structural Dynamics 3 (January) (1974) 121–138.

URL http://onlinelibrary.wiley.com/doi/10.1002/eqe.4290030203/abstract

[20] S. Gajan, P. Raychowdhury, T. C. Hutchinson, B. L. Kutter, J. P. Stewart, Application and validation of practical tools for nonlinear soil-foundation interaction analysis, Earthquake Spectra 26 (1) (2010) 111–129. doi:10.1193/1.3263242.

[21] ATC, A practical guide to soil-structure interaction, Tech. Rep. FEMA P-2091, Applied Technology Council, Redwood Shores, CA; Federal Emergency Management Agency, Washington DC, USA (2020).

[22] A. Pais, E. Kausel, Approximate formulas for dynamic stiffnesses of rigid foundations, Soil Dynamics and Earthquake Engineering 7 (4) (1988) 213–227. doi:10.1016/S0267-7261(88)80005-8.

[23] C.-H. Loh, W.-Y. Jean, J. Penzien, Uniform-hazard response spectra—an alternative approach, Earthquake Engineering & Structural Dynamics 23 (4) (1994) 433–445. doi:10.1002/eqe.4290230406.
URL https://onlinelibrary.wiley.com/doi/abs/10.1002/eqe.4290230406

[24] E. Kausel, R. V. Whitman, J. P. Morray, F. Elsabee, The spring method for embedded foundations, Nuclear Engineering and Design 48 (2-3) (1978) 377–392. doi:10.1016/0029-5493(78)90085-7.

[25] D. Vamvatsikos, C. Allin Cornell, Incremental dynamic analysis, Earthquake Engineering and Structural Dynamics 31 (3) (2002) 491–514. doi:10.1002/eqe.141.

[26] V. Silva, N. Horspool, Combining USGS ShakeMaps and the OpenQuake-engine for damage and loss assessment, Earthquake Engineering and Structural Dynamics (August 2016) (2019) 1–19.

[27] A. Miano, F. Jalayer, H. Ebrahimian, A. Prota, Cloud to IDA: Efficient fragility assessment with limited scaling, Earthquake Engineering and Structural Dynamics 47 (5) (2018) 1124–1147.

[28] M. Kohrangi, D. Vamvatsikos, P. Bazzurro, Pulse-like versus non-pulse-like ground motion records: Spectral shape comparisons and record selection strategies, Earthquake Engineering & Structural Dynamics 48 (1) (2019) 46–64. doi:10.1002/eqe.3122.

[29] G. Baltzopoulos, R. Baraschino, I. Iervolino, On the number of records for structural risk estimation in PBEE, Earthquake Engineering & Structural Dynamics 48 (5) (2018) eqe.3145. doi:10.1002/eqe.3145.
URL https://onlinelibrary.wiley.com/doi/10.1002/eqe.3145

[30] A. J. Kappos, G. Panagopoulos, C. Panagiotopoulos, G. Penelis, A hybrid method for the vulnerability assessment of R/C and URM buildings, Bulletin of Earthquake Engineering 4 (4) (2006) 391–413. doi:10.1007/s10518-006-9023-0.

[31] L. Martins, V. Silva, H. Crowley, F. Cavalieri, Vulnerability modellers toolkit, an open-source platform for vulnerability analysis, Bulletin of Earthquake Engineering 19 (13) (2021) 5691–5709. doi:10.1007/s10518-021-01187-w.

[32] S. Mazzoni, F. McKenna, M. H. Scott, G. L. Fenves, Open system for earthquake engineering simulation user command-language manual, Tech. Rep. Pacific Earthquake Engineering Research Center, Berkeley, USA (2009).

[33] D. C. Kent, R. Park, Inelastic behavior of reinforced concrete members with cyclic loading, Bulletin of the New Zealand Society for Earthquake Engineering 4 (1971) 108–125.

[34] B. D. Scott, R. Park, M. J. N. Priestley, Stress-Strain Behavior of Concrete Confined by Overlapping Hoops at Low and High Strain Rates (1982).

[35] I. Karsan, J. Jirsa, Behavior of concrete under compressive loadings, Journal of the Structural Division 95 (1969) 2535–2563.

[36] G. A. Chang, J. B. Mander, Seismic Energy Based Fatigue Damage Analysis of Bridge Columns : Part 1 - Evaluation of Seismic Capacity, NCEER Technical Report No. NCEER-94-0006 (1994) 230doi:TechnicalReportNCEER-94-0006.

[37] J. Stewart, G. Fenves, R. Seed, Seismic soil-structure interaction in buildings. i: Analytical methods, Journal of Geotechnical and Geoenvironmental Engineering 125 (1) (1999) 26–37.

[38] P. Raychowdhury, T. C. Hutchinson, Performance evaluation of a nonlinear Winkler-based shallow foundation model using centrifuge test results, Earthquake Engineering and Structural Dynamics 38 (5) (2009) 679–698. arXiv:1403.5481, doi:10.1002/eqe.902.

[39] G. Mylonakis, S. Nikolaou, G. Gazetas, Footings under seismic loading: Analysis and design issues with emphasis on bridge foundations, Soil Dynamics and Earthquake Engineering 26 (9) (2006) 824–853. doi:10.1016/j.soildyn.2005.12.005.

[40] EN-1998, Eurocode 8: Design of structures for earthquake resistance 3 (2005).

[41] J. Lysmer, A. M. Kuhlemeyer, Finite dynamic model for infinite media, Journal of the Engineering Mechanics Division 95 (1969) 859–877.

[42] Federal Emergency Management Agency, Seismic Performance Assessment of Buildings - methodology, Fema P-58-1 1 (September) (2012) 278.

[43] D. D'Ayala, A. Meslem, D. Vamvatsikos, K. Porter, T. Rossetto, H. Crowley, V. Silva, Guidelines for Analytical Vulnerability Assessment - Low/Mid-Rise, GEM Technical Report 08 (2013) 162.

[44] R. Tomeo, D. Pitilakis, A. Bilotta, E. Nigro, SSI effects on seismic demand of reinforced concrete moment resisting frames, Engineering Structures 173 (June) (2018) 559–572. doi:10.1016/j.engstruct.2018.06.104.

[45] T. Rossetto, A. Elnashai, Derivation of vulnerability functions for European-type RC structures based on observational data, Engineering Structures 25 (10) (2003) 1241–1263. doi:10.1016/S0141-0296(03)00060-9.

[46] A. Ghobarah, On drift limits associated with different damage levels, International workshop on performance-based seismic design concepts and implementation (February) (2004) 321–332.
URL http://peer.berkeley.edu/publications/peer{_}reports/reports{_}2004/reports{_}2004.html

[47] FEMA-NIBS, Multi-hazard loss estimation methodology: Earthquake model: Hazus mh technical manual, Tech. Rep. Pacific Earthquake Engineering Research Center, Washington, DC, USA (2004).

[48] K. Pitilakis, E. Riga, A. Anastasiadis, S. Fotopoulou, S. Karafagka, Towards the revision of ec8: Proposal for an alternative site classification scheme and associated intensity dependent spectral amplification factors, Soil Dynamics and Earthquake Engineering 126 (2019) 105137. doi:https://doi.org/10.1016/j.soildyn.2018.03.030.

[49] P. Raychowdhury, Seismic response of low-rise steel moment-resisting frame (smrf) buildings incorporating nonlinear soil-structure interaction (ssi) 33 (3) (2011) 958–967.

[50] D. Pitilakis, E. Rovithis, A. Anastasiadis, A. Vratsikidis, M. Manakou, Field evidence of SSI from full-scale structure testing, Soil Dynamics and Earthquake Engineering 112 (March) (2018) 89–106. doi:10.1016/j.soildyn.2018.04.024.
URL https://doi.org/10.1016/j.soildyn.2018.04.024